

FULL PAPER

Electrical properties and ^{18}O tracer diffusion in $(\text{Bi}_{0.5}\text{Na}_{0.5})\text{TiO}_3$ ceramics doped with CuO and Nb_2O_5

Kanaka Iwasaki¹, Yuka Takagi^{1,†}, Hyunwook Nam¹, Hajime Nagata¹ and Isao Sakaguchi²

¹Tokyo University of Science, 2641 Yamazaki, Noda, Chiba 278–8510, Japan

²National Institute for Materials Science, 1–1 Namiki, Tsukuba, Ibaraki 305–0044, Japan

$(\text{Bi}_{0.5}\text{Na}_{0.5})\text{TiO}_3$ [BNT] ceramics can be sintered at low temperatures of 940 °C with CuO addition. This is believed to reduce Bi^{3+} volatilization and improve the quality of BNT-based ceramics by lowering the number of oxygen vacancies. However, there is no direct evidence that low-temperature sintering prevents the formation of oxygen vacancies. In this study, the formation of oxygen vacancies by ^{18}O tracer diffusion and the additive effect of CuO on this formation in BNT ceramics were examined using secondary ion mass spectrometry (SIMS). In addition, Nb_2O_5 , which acts as a donor, was added to the CuO -doped BNT ceramics. The formation of oxygen vacancies was discussed, and the electrical properties were clarified. As a result, the volume diffusion coefficients D of the BNT ceramics with 0.5 wt % CuO ($\text{Cu}0.5$) were $2.0 \times 10^{-11} \text{ cm}^2/\text{s}$. This value is equivalent to pure BNT, which means that for BNT ceramics, CuO acts as an acceptor, suggesting that BNT ceramics still contain many oxygen vacancies. On the other hand, the D of ^{18}O in $\text{Cu}0.5$ added 0.4 wt % Nb_2O_5 was $3.5 \times 10^{-15} \text{ cm}^2/\text{s}$, indicating that the formation of oxygen vacancies is suppressed. Moreover, Nb_2O_5 enhanced the poling treatment and the coercive field E_c decreased, indicating a softening trend.

Key-words : Lead-free piezoelectric ceramics, $\text{Bi}_{0.5}\text{Na}_{0.5}\text{TiO}_3$, Nb_2O_5 donor additive, ^{18}O tracer diffusion

[Received January 7, 2025; Accepted April 18, 2025; Published online May 20, 2025]

1. Introduction

In recent years, lead-free piezoelectric materials have garnered considerable attention as environmentally friendly substitutes for lead-containing materials. Perovskite-structured lead-free piezoelectric materials, in particular, are well-suited for use in actuators and high-power devices.^{1,2)} $(\text{Bi}_{0.5}\text{Na}_{0.5})\text{TiO}_3$ (BNT) ceramics are considered promising lead-free piezoelectric materials due to their relatively low production costs and excellent piezoelectric characteristics.^{3–16)} Generally, BNT ceramics are known to have the highest relative density when sintered at 1140 °C. However, secondary ion mass spectrometry (SIMS) analysis has revealed significant Bi^{3+} ion volatilization near 1100 °C, raising concerns about potential compositional instability.¹⁷⁾ Therefore, the BNT ceramics must be sintered at low temperatures. However, their d_{33} values are relatively smaller compared to those of PZT-based ceramics. To address this limitation, incorporating multilayer structures has proven highly effective for actuators and high-power devices, as the overall displacement scales with the number of layers. In the case of $(\text{K},\text{Na})\text{NbO}_3$ -based ceramics, the multilayer ceramic actuators (MLCAs)

utilizing inner Ni electrodes have demonstrated outstanding piezoelectric performance.^{18,19)} However, Bi-based ceramic MLCAs cannot be manufactured using base metal electrodes like Ni. This is because the partial pressure of oxygen ($p\text{O}_2$) levels for the $\text{Bi}/\text{Bi}_2\text{O}_3$ system fall within the range of 10^{-10} to 10^{-12} atm, which are consistently higher than those of the Ni/NiO system across all temperatures, as indicated by the Ellingham diagram.²⁰⁾ In other words, Bi-based oxide ceramics are more easily reduced than Ni electrodes. Therefore, the ceramics cannot be sintered in a reducing atmosphere without the Ni oxidation. Consequently, the fabrication of Bi-based MLCAs requires using precious metals such as Ag, Pt, and Ag–Pd.

Typically, Ag–Pd electrodes are commonly utilized in PZT-based MLCAs due to their cost-effectiveness. The melting point of Ag–Pd alloys decreases as the proportion of costly Pd is reduced.²¹⁾ Recently, a 95:5 Ag–Pd ratio has been employed in the production of PZT-based MLCAs, necessitating a sintering temperature below 990 °C. Similarly, Ag–Pd electrodes have also been used as internal electrodes in fabricating MLCAs from BNT-based ceramics.²²⁾ At co-sintering temperatures of around 1100–1130 °C, the Ag–Pd electrodes were not fully activated, leading to a reduction in the electrical performance of the MLCA compared to bulk ceramics. Furthermore, the diffusion behavior of Ag used as an electrode material was analyzed through SIMS.²³⁾ The diffusion of Ag at the grain boundaries significantly affected the chemical and physical

[†] Corresponding author: Y. Takagi; E-mail: y-takagi@rs.tus.ac.jp

[‡] Preface for this article: DOI <https://doi.org/10.2109/jcersj2.133.P7-1>

strengths of the grain boundaries of the BNT ceramics. The diffusion coefficient at the grain boundaries in BNT ceramics is comparable to that of Pb-based ceramics.^{24,25)} These reports indicate that low-temperature sintering of BNT based ceramics is essential for the co-sintering of internal electrodes and BNT-based ceramics.

CuO is commonly employed as a sintering aid owing to its low melting point and ability to form a liquid-phase in both BNT-based ceramics^{26–40)} and $(\text{K},\text{Na})\text{NbO}_3$ (KNN)-based ceramics.^{41–47)} The presence of the liquid-phase greatly improves mass transport along grain boundaries, leading to increased final densities. In particular, sintering aids can diffuse into ceramics and negatively affected their properties.⁴⁸⁾ Moreover, an excessive amount of CuO may lead to abnormal grain growth driven by the liquid-phase,⁴⁹⁾ which can further deteriorate piezoelectric performance,^{50,51)} similar to what is observed in KNN. Therefore, it is essential to minimize the concentration of sintering aids. In addition, effective densification at low temperatures requires strong adhesion between the liquid-phase and ceramic particles. A high surface tension is required between the liquid-phase and the particles, which is reflected by a low contact angle.⁵²⁾ However, determining the contact angle of the liquid-phase is challenging, as it must be measured experimentally at the sintering temperature.⁵³⁾ In our previous study, we prepared BNT ceramics doped with 1.0 wt % CuO ($\text{BNT} + \text{CuO}$), and clarified their electrical properties and low-temperature sintering mechanisms. The role of CuO were clarified as causing the formation of a liquid-phase of compounds of Cu , Na , Ti , and O ions (NCT). The sintering of BNT ceramics was achieved at 940°C , which is 200°C lower than 1140°C .⁵⁴⁾ Low temperature sintering at 940°C by CuO doping can suppress the Bi vaporization during the sintering, leading to the suppression of formation of oxygen vacancies. However, no direct results have been reported showing that low-temperature sintering suppresses the formation of oxygen vacancies. Moreover, the same average grain size of the $\text{BNT} + \text{CuO}$ as that of pure BNT was realized at a sintering temperature 200°C lower than that of the pure BNT ceramics. Thus, it is assumed that the addition of CuO promoted grain growth. This grain growth is attributed to the enhanced diffusion of oxygen vacancies. When the Ti^{4+} -site of BNT perovskite structure is replaced by Cu^{2+} ions, they have the potential to act as acceptors. However, the role of CuO as a dopant and the number of oxygen vacancies in $\text{BNT} + \text{CuO}$ have not been clarified. Furthermore, the concentration of oxygen vacancies, as measured by ^{18}O tracers using SIMS, decreases in BNT ceramics with the addition of 0.4 wt % Nb_2O_5 .¹⁴⁾ This reduction is attributed to the substitution of Ti^{4+} sites by Nb^{5+} in the BNT perovskite structure. Furthermore, the addition of Nb_2O_5 increases the resistivity of BNT ceramics, while at the same time reducing the coercive force (E_c), showing a softening tendency. In other words, Nb_2O_5 effectively suppresses the formation of oxygen vacancies and acts as a donor in BNT ceramics.¹⁴⁾ Therefore, if Cu^{2+} ions are acting as acceptors in BNT ceramics, it is expected that co-doping with Nb^{5+}

ions will be effective in suppressing the formation of oxygen vacancies. In this study, we examined the formation of oxygen vacancies via ^{18}O tracer diffusion in CuO -doped BNT ceramics using secondary ion mass spectrometry (SIMS). In addition, the number of oxygen vacancies in BNT ceramics with co-doped, CuO and Nb_2O_5 , was discussed using ^{18}O tracer diffusion, and the electrical properties were evaluated.

2. Experimental

$(\text{Bi}_{0.5}\text{Na}_{0.5})\text{TiO}_3 + x\text{CuO}$ ($x = 0, 0.5, 1.0$ wt %, Cu_x) and $\text{BNT} + \text{Cu}_x + y\text{Nb}_2\text{O}_5$ ($y = 0, 0.2, 0.4, 0.8, 1.0$ wt %, $\text{Cu}_x + \text{Nb}_y$) ceramics were prepared using conventional ceramic fabrication techniques. The starting materials were mixed in ethanol via ball milling with zirconia balls for 20 h. After drying, the mixed powder was calcined in an alumina crucible at 850°C for 2 h. Nb_2O_5 was added to the calcined powder of Cu_x . The calcined powder was re-ground via ball milling for 20 h, then pressed into pellets with a diameter of 20 mm and a thickness of 10 mm using a uniaxial press. The pellets were subsequently treated with cold isostatic pressing at 150 MPa. Each sample was sintered at 940°C for 2 h. The ceramic densities were determined using Archimedes method. The crystal structure and lattice parameters of the bulk samples were analyzed using X-ray diffraction (XRD, Rigaku RINT-2000, 40 kV, 40 mA) with $\text{Cu-K}\alpha$ radiation. By using the results of XRD, the lattice distortion $90-\alpha$ was obtained. Here, the α (α) value was determined by numerically solving the following equation.

$$\frac{1}{d^2} = \frac{(h^2 + k^2 + l^2) \sin^2 \alpha + 2(hk + kl + hl)(\cos^2 \alpha - \cos \alpha)}{a^2(1 - 3 \cos^2 \alpha + 2 \cos^3 \alpha)} \quad (1)$$

In this equation, d is the interplanar spacing measured with XRD, and (h, k, l) are Miller indices.

An Ag electrode was applied to the ceramic surface for measuring its piezoelectric properties as well as the resistivity. The resistivity was determined by RA/t , where R was the resistance measured with High-Resistance Meter (YHP 4339B) made by Keysight Technologies, Inc., and A and t are the area and thickness of the electrode that has the diameter of 10 mm and the thickness of 0.5 mm. Longitudinal vibration in the (33) mode was evaluated using rectangular specimens with dimensions $2\text{ mm} \times 2\text{ mm} \times 5\text{ mm}$. The samples were poled in a silicone oil bath under a DC electric field of 5 kV/mm for 5 min at room temperature, then assessed using the resonance-antiresonance method as per IEEE standards with an impedance analyzer (HP4294A). The P - E hysteresis loops were measured using a virtual ground system (Toyo Corporation, Model 6252 Rev. C) at room temperature and 10 Hz. The ^{18}O concentration profile was analyzed using a SIMS system (Cameca IMS-4F) at the National Institute for Materials Science, Japan. A $^{133}\text{Cs}^+$ beam accelerated at 10 kV was used as the primary ion to irradiate the sample surface. The

primary beam was scanned in a raster pattern over a $100 \times 100 \mu\text{m}^2$ area. A Cameca normal-induced electron gun was used to stabilize the surface potential during $^{133}\text{Cs}^+$ irradiation. A dynamic transfer system defined the measurement area of secondary ions and the raster window ranging from 40 to 50 %. The secondary ions, $^{16}\text{O}^-$ (reference mass), and $^{18}\text{O}^-$, from this area were detected using an electron multiplier. The ^{18}O tracers were diffused by annealing the samples at 450°C for 30 min in an ^{18}O atmosphere. The concentration profile was calculated from the oxygen intensities as follows:

$$C = \frac{I(^{18}\text{O})}{I(^{18}\text{O}) + I(^{16}\text{O})} \quad (2)$$

where $I(^{16}\text{O})$ and $I(^{18}\text{O})$ are the intensities of ^{16}O and ^{18}O peaks, respectively. The volume diffusion contribution in the profile was fitted to the diffusion equation for a constant concentration at the surface as follows:

$$\frac{C_x - C_{\text{bg}}}{C_s - C_{\text{bg}}} = \text{erfc}\left(\frac{x}{2\sqrt{Dt}}\right) \quad (3)$$

where C_x is the ^{18}O concentration at depth x , C_s is the surface concentration of ^{18}O , and C_{bg} is the natural background abundance of ^{18}O . Equation (2) assumes an equilibrium between the crystal surface and gas phase and thus a constant C_s value. D and t are the volume diffusion coefficient and annealing time, respectively.

3. Results and discussion

3.1 Effect of CuO on oxygen vacancies formation

Figure 1 shows the ^{18}O tracer diffusion profiles of Cu0.5, which were compared with the profiles of BNT ceramics with no additives (pure BNT), MgO 0.4 wt % (Mg0.4), and Nb₂O₅ 0.4 wt % (Nb0.4). The volume diffusion coefficients D of Cu0.5 were $2.0 \times 10^{-11} \text{ cm}^2/\text{s}$. This value is equivalent to that of pure BNT, $2.5 \times 10^{-11} \text{ cm}^2/\text{s}$. BNT ceramics were originally p-type and have recently become known as ionic conductors,⁵⁵⁾ which means that many oxygen vacancies are present in BNT ceramics. Thus, Cu0.5 was assumed to contain many oxygen vacan-

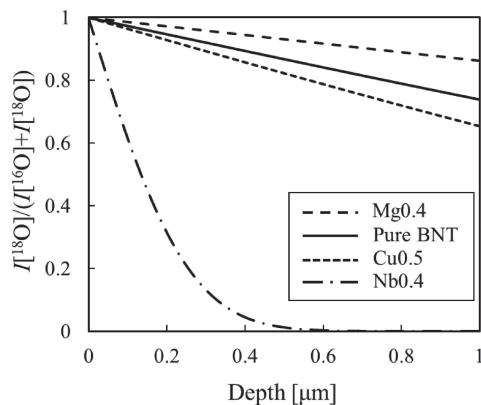


Fig. 1. ^{18}O tracer diffusion profiles of pure BNT, Cu0.5, Mg0.4, and Nb0.4 after annealing at 450°C for 30 min.

cies. Moreover, in our previous study, the D of Mg0.4, and Nb0.4 exhibits 9.2×10^{-11} and $1.1 \times 10^{-13} \text{ cm}^2/\text{s}$, respectively.¹⁴⁾ It is suggested that this large difference in D values is due to substituting of Ti^{4+} sites by Mg^{2+} and Nb^{5+} ions, i.e., the difference in the number of oxygen vacancies as ^{18}O tracer diffusion. The additives MgO and Nb₂O₅ act as an acceptor and donor, for BNT ceramics.¹⁷⁾ This means that the value of D can indicate of the amount of oxygen vacancies. The D value of the BNT ceramics with Cu0.5 was similar to that of the BNT ceramics with Mg0.4. Thus, CuO behaved as an acceptor for BNT ceramics because Cu^{2+} ions replaced the Ti^{4+} sites. As shown in our previous study, Cu0.5 can be sintered at a low temperature of 940°C .¹⁶⁾ The low-temperature sintered CuO-doped BNT ceramics are believed to suppress the volatilization of Bi^{3+} ions from around 1100°C , thus avoiding the formation of oxygen vacancies. However, CuO-doped BNT ceramics contain large numbers of oxygen vacancies even when sintered at low temperatures. Based on these results, Nb₂O₅ is added to the CuO-doped BNT ceramics to suppress the formation of oxygen vacancies. In the next section, we discuss the oxygen diffusion and electrical properties of the CuO-doped BNT ceramics with added Nb₂O₅.

3.2 CuO-doped BNT ceramics with added Nb₂O₅

Figure 2 shows the XRD patterns of Pure BNT, Cu0.5, Cu1.0, Nb0.4, Cu0.5 + Nb0.4, and Cu1.0 + Nb0.4. The XRD pattern shows a rhombohedral perovskite structure, with a detailed observation showing a peak at approximately 34° . This peak was attributed to the liquid-phase NCT formed by adding of CuO. The relative density of $\text{Cu}_x + \text{Nb}_y$ ($x = 0.5, 1.0 \text{ wt } \%, y = 0, 0.2, 0.4, 0.8, 1.0 \text{ wt } \%$) averaged 98 % as shown in **Fig. 3(a)**. The lattice constants for these samples averaged 3.89 \AA , and these values did not change significantly for any CuO and Nb₂O₅ content as shown in **Fig. 3(b)**. Furthermore, **Fig. 3(c)** shows the lattice distortion $90-\alpha$ as a function of the amount of Nb₂O₅ in y phase. The $90-\alpha$ of the samples did not change significantly until the addition of 0.2 wt % Nb₂O₅. On the other hand, the $90-\alpha$ value of the samples

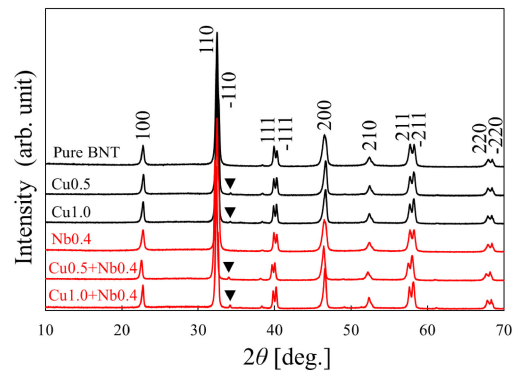


Fig. 2. XRD patterns of Pure BNT, Cu0.5, Cu1.0, Nb0.4, Cu0.5 + Nb0.4, and Cu1.0 + Nb0.4. (The peak at approximately 34° was attributed to the liquid-phase NCT formed by adding of CuO).

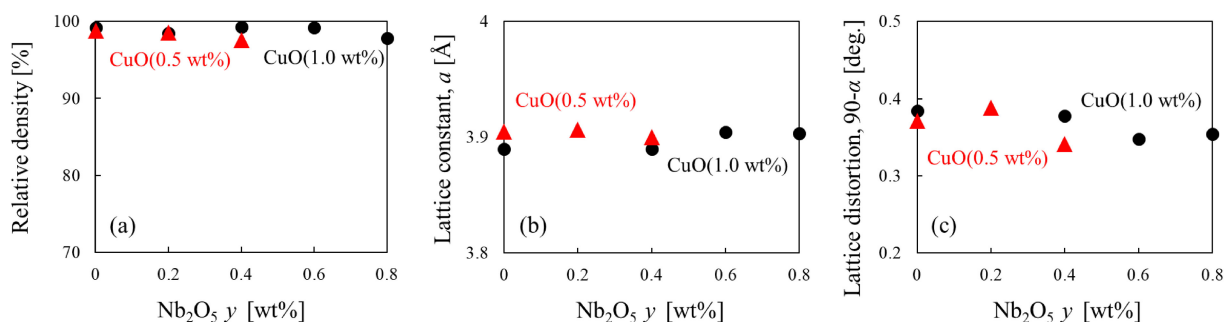


Fig. 3. (a) Relative densities, (b) Lattice constants a , and (c) lattice distortion $90-\alpha$ for pure BNT, $\text{Cu}_x + \text{Nb}_y$ ($x = 0.5, 1.0$ wt%, $y = 0, 0.2, 0.4, 0.8, 1.0$ wt%).

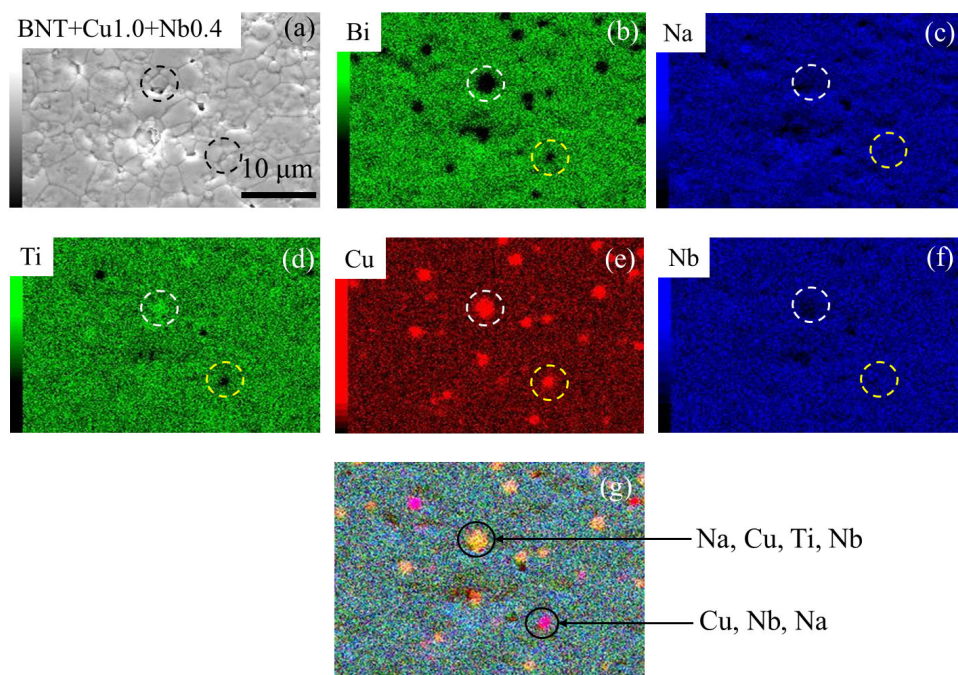


Fig. 4. (a) SEM image of the grains, (b)–(f) mapping of each element, such as Na, Bi, Ti, Cu, and Nb ions, and (g) overlay of the elemental maps.

with 0.4% or more of Nb_2O_5 added decreased slightly. However, these changes are not sufficiently pronounced to cause a change in the lattice constant, as shown in Fig. 3(b).

Figure 4(a) shows the SEM image of the grains. The mapping of each element, such as Na, Bi, Ti, Cu, and Nb ions, is shown in Figs. 4(b)–4(f) and Fig. 4(g) is an overlay of the elemental maps. A Cu-based grain was identified at the triple points of the grains. While Na^+ , Ti^{4+} , and Nb^{5+} ions were found within the Cu-based grains, as highlighted by white dashed circles, Bi ions were absent. Furthermore, in Cu-based grains, grains with and without Ti ions were observed as shown in Fig. 4(g). Hence, it is proposed that the Cu-based grains consist of compounds containing Cu, Na, Ti, Nb, and O ions instead of only Cu. A closer inspection of the XRD pattern in Fig. 2 reveals a peak near 34° . This peak closely resembles that of $\text{NaCu}_{2.5}\text{Ti}_{4.5}\text{O}_{12}$ (PDF No. 01-078-5412, referred to as NCT).⁵⁴⁾ It has been documented that compounds containing Cu and Ti,⁵⁶⁾ as well as those with Cu and Na⁵⁷⁾, can

lower the melting point. The melting point of Cu-based grain was therefore reduced when combined with Na and Ti. This indicates that NCT forms a liquid-phase during sintering due to its lowered melting point. Furthermore, the addition of Nb suggests that Nb is also incorporated into the liquid-phase NCT. Therefore, it is suggested that there are both Nb^{5+} ions contained in the liquid-phase and those that replace the B-site of BNT.

Figure 5 shows the ^{18}O tracer diffusion profile of $\text{Cu}0.5 + \text{Nb}0.4$, which was compared to those of pure BNT and $\text{Cu}0.5$. The D of ^{18}O in $\text{Cu}0.5 + \text{Nb}0.4$ was $3.5 \times 10^{-15} \text{ cm}^2/\text{s}$ and this value is slower than that of $\text{Cu}0.5$. This indicates that the addition of the donor Nb^{5+} ions suppressed the formation of oxygen vacancies in $\text{Cu}0.5$. Low-temperature sintering and reduced oxygen vacancies were achieved for $\text{Cu}0.5 + \text{Nb}0.4$. In addition, the SEM images of the grains of $\text{Cu}0.5$ and $\text{Cu}0.5 + \text{Nb}0.4$ are shown in **Figs. 6(a)–6(b)** and **6(c)–6(d)**, respectively. The average grain sizes of these were 5.53 and 2.74 μm , respectively. As shown in previous reports, the grain

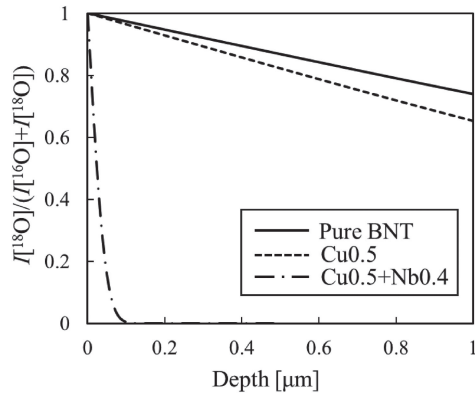


Fig. 5. ^{18}O tracer diffusion profile of pure BNT, Cu0.5, and Cu0.5 + Nb0.4 after annealing at 450 °C for 30 min.

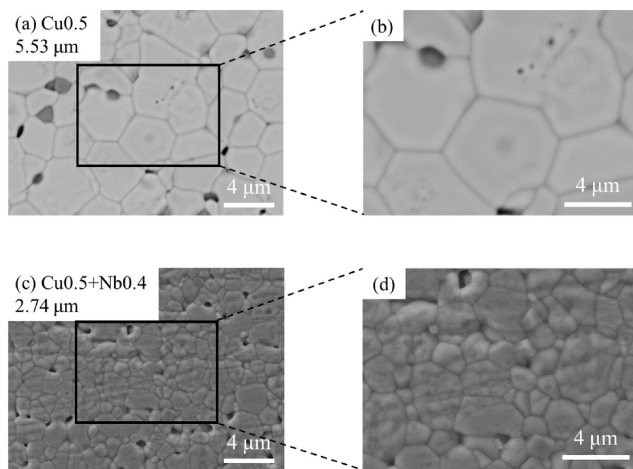


Fig. 6. SEM images of grain structures and average grain sizes for (a), (b) Cu0.5 and (c), (d) Cu0.5 + Nb0.4. (e) Average grain sizes of $\text{Cu}_x + \text{Nb}_y$ ($x = 0.5, 1.0$ wt %) as a function of the amount of Nb_2O_5 y .

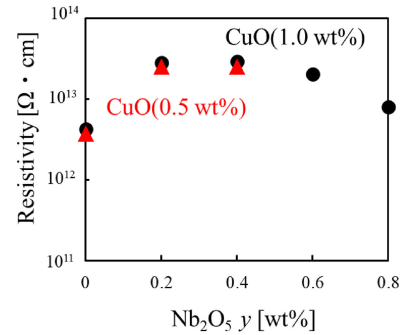
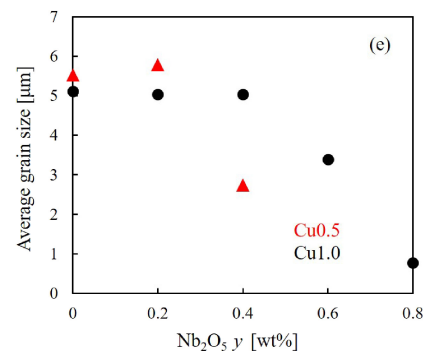


Fig. 7. Resistivity ρ of Cu0.5 and Cu1.0 as a function of the amount of Nb_2O_5 y .



size of Cu0.5 was larger than that of pure BNT ceramics ($4.18\mu\text{m}$).⁵⁴⁾ This is because the grain grew due to the diffusion of oxygen vacancies, as shown in Fig. 5. In contrast, for Cu0.5 + Nb0.4, the formation of oxygen vacancies is suppressed, and as a result, grain growth is inhibited. The average grain sizes of Cu0.5 and Cu1.0 with respect to the amount of Nb_2O_5 added is summarized in Fig. 6(c). The average grain size decreased as the amount of Nb_2O_5 added increased. Therefore, the grain growth observation also showed that adding of Nb suppressed the formation of oxygen vacancies.

To determine the optimum amount of Nb_2O_5 , the amount of Nb_2O_5 added was controlled for the Cu0.5 and Cu1.0. Figure 7 shows resistivity ρ as a function of doped the Nb_2O_5 amount of y . The ρ showed a maximum value of $10^{13}\Omega\text{cm}$ at $y = 0.4$. This value is comparable for both Cu0.5 and Cu1.0. Since BNT is originally p-type, the addition of the donor Nb_2O_5 caused the charge to approach neutrality, thus increasing ρ . Previously, a trend of increasing resistivity was observed for Nb0.4.¹⁴⁾ For values of x greater than 0.4, the ρ decreased. This suggested that the number of Nb^{5+} ions was too high to act effectively as donors. Thus, approximately 0.4 wt % Nb_2O_5 was assumed to be optimal in this system.

The P - E hysteresis loops of pure BNT, Cu1.0 and Cu1.0 + Nb0.4 at room temperature and 10 Hz were shown in Fig. 8(a). The loops were fully saturated and exhibited good rectangularities. The coercive electric field E_c values of pure BNT, Cu1.0, and Cu1.0 + Nb0.4 were 74.8, 75.7, and 69.7 kV/cm, respectively. The E_c of Cu1.0 was not significantly different from that of pure BNT, while the E_c of Cu1.0 + Nb0.4 was lower than those of Cu1.0 and pure BNT. Figure 8(b) shows the E_c of Cu1.0 with respect to the amount of Nb_2O_5 added. E_c decreased as the amount of Nb_2O_5 added increased. In other words, a softening trend is observed with the addition of Nb_2O_5 , indicating that the formation of oxygen vacancies is suppressed. This is also consistent with the fact that CuO addition alone does not suppress the formation of oxygen vacancies, as shown in Fig. 1. The softening trend shown in Fig. 8 is also consistent with the relationship between the softening (or hardening) trend and the decrease (or increase) in the oxygen vacancies shown in Ref. 14. In this reference,¹⁴⁾ the softening trend induced with the addition of only Nb_2O_5 without CuO addition. In the same reference,¹⁴⁾ the hardening trend with the addition of only MgO is shown to be induced by the increase in oxygen vacancies.

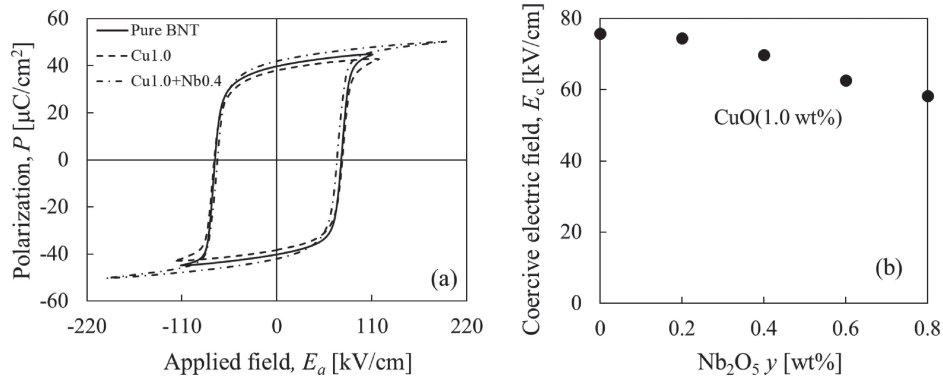


Fig. 8. (a) P - E hysteresis loops were compared among pure BNT, Cu1.0 and Cu1.0 + Nb0.4 at room temperature and 10 Hz. (b) Relationship between E_c and the amount of Nb_2O_5 y.

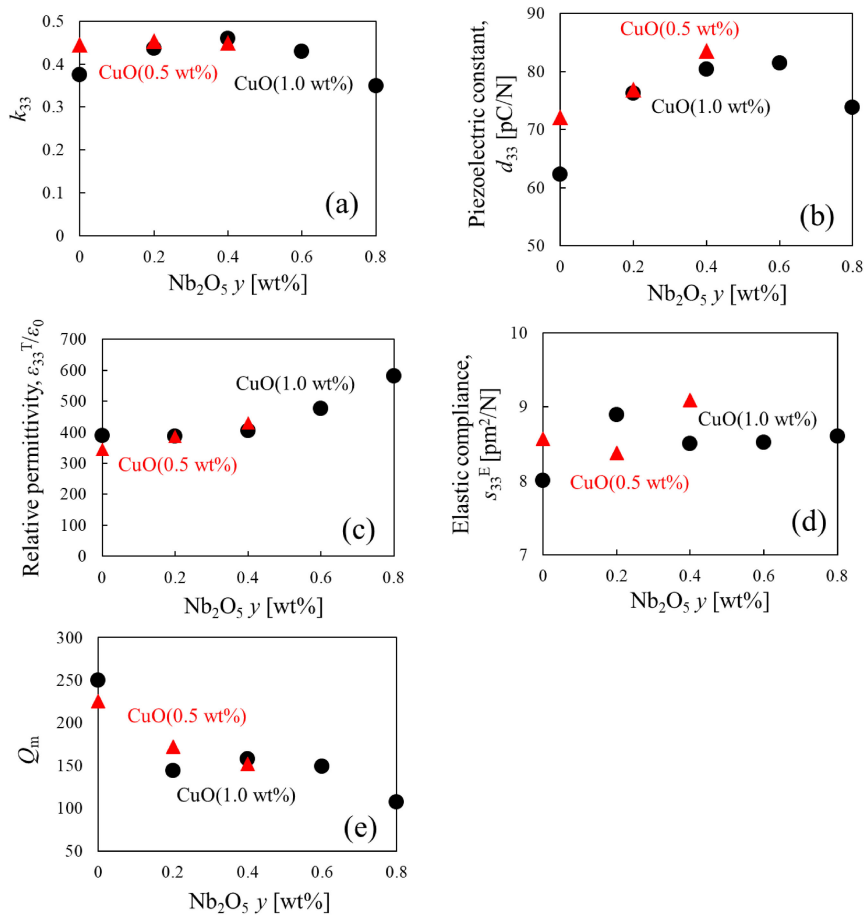


Fig. 9. Piezoelectric properties (a) k_{33} , (b) d_{33} , (c) $\epsilon_{33}^T/\epsilon_0$, (d) s_{33}^E , and (e) Q_m of Cu0.5 and Cu1.0 as functions of the amount of Nb_2O_5 y.

Figure 9 shows the piezoelectric properties (a) the electromechanical coupling factor k_{33} , (b) the piezoelectric constant d_{33} (c) the relative free permittivity $\epsilon_{33}^T/\epsilon_0$, (d) the elastic compliance s_{33}^E , and (e) the mechanical quality factor Q_m as functions of the amount of Nb_2O_5 y. k_{33} shows a maximum value of 0.43 at $y = 0.4$ for both Cu0.5 and Cu1.0, which is almost the same as the value for pure BNT. Also, d_{33} shows a maximum value of 83.6 pC/N at $y = 0.4$ for Cu0.5. d_{33} increased at $y = 0.4$ compared to $y = 0$ for Cu0.5 and Cu1.0. This is because, the addition

of Nb_2O_5 reduces oxygen vacancies as shown in Fig. 5; therefore, the domain pinning effect is smaller, and polarization inversion is easier. $\epsilon_{33}^T/\epsilon_0$ are maintained at approximately 400, independent of the amount of Nb_2O_5 added. For Cu1.0 + Nb0.8, the values of $\epsilon_{33}^T/\epsilon_0$ shows approximately 600 which means that θ_{\max} was 76° , which indicating that polarization inversion did not proceed. Moreover, s_{33}^E increased and Q_m decreased with the addition of Nb_2O_5 addition as shown in Figs. 9(d) and 9(e), respectively. This indicates that the samples are softened

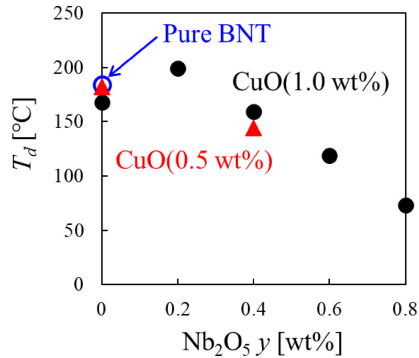


Fig. 10. T_d as a function of the amount of Nb_2O_5 , y .

both materially and electrically, and this is due to the suppression of the formation of oxygen vacancies. In other words, the domain pinning effect of the oxygen vacancies was small.

Figure 10 shows the depolarization temperature T_d of $\text{Cu}_x + \text{Nb}_y$ ($x = 0.5, 1.0 \text{ wt\%}$, $y = 0, 0.2, 0.4, 0.8, 1.0 \text{ wt\%}$) as a function of the amount of Nb_2O_5 . In the case of $y = 0$, the addition of Cu causes the T_d to decrease by about 10°C compared to pure BNT which is consistent with the previous report.⁵⁴⁾ Furthermore, the addition of Nb tended to reduce T_d further. The tendency of T_d to decrease with the addition of Nb_2O_5 is consistent with a previous report.¹⁴⁾ However, the T_d of Cu0.5 sintered at 940°C is around 170°C , while the T_d increases to around 190°C due to the quenching effect.⁸⁻¹⁶⁾ Thus, applying the quenching effect makes it possible to increase T_d of $\text{Cu}_x + \text{Nb}_y$.

4. Conclusion

While the addition of only Nb_2O_5 showed no effect of suppressing Bi^{3+} volatilization with only the effect of suppressing oxygen vacancies in the previous studies, the addition of only CuO showed little effect of suppressing oxygen vacancies with only the effect of suppressing Bi^{3+} volatilization due to the lowered sintering temperature. In this study, the number of oxygen vacancies for ^{18}O tracer diffusion was evaluated by SIMS for CuO-doped BNT ceramics with Nb_2O_5 as a donor additive; subsequently their electrical properties were examined. Consequently, in CuO-doped BNT ceramics with Nb_2O_5 , oxygen vacancies and Bi^{3+} volatilization were simultaneously suppressed. The addition of Nb_2O_5 resulted in softening tendency and improved the piezoelectric properties. These approaches can guide fabricating high-quality BNT ceramics with suppressed oxygen vacancies.

References

- 1) T. Takenaka, H. Nagata, Y. Hiruma and K. Matsumoto, *J. Electroceram.* **19**, 259 (2007).
- 2) S. E. Park and T. R. Shrout, *IEEE T. Ultrason. Ferr.* **44**, 1141 (1997).
- 3) T. Takenaka and H. Nagata, *J. Eur. Ceram. Soc.* **12**, 2693 (2005).
- 4) H. Nagata, N. Koizumi, N. Kuroda, I. Igarashi and T. Takenaka, *Ferroelectrics* **229**, 273 (1999).
- 5) L. Liu and H. Fan, *J. Electroceram.* **16**, 293 (2006).
- 6) H. Nagata, *J. Ceram. Soc. Jpn.* **116**, 271 (2008).
- 7) T. Hoshina, Y. Kigoshi, T. Furuta, H. Takeda and T. Tsurumi, *Jpn. J. Appl. Phys.* **50**, 09NC07 (2011).
- 8) H. Muramatsu, H. Nagata and T. Takenaka, *Jpn. J. Appl. Phys.* **55**, 10TB07 (2016).
- 9) T. Miura, H. Nagata and T. Takenaka, *Jpn. J. Appl. Phys.* **56**, 10PD05 (2017).
- 10) H. Nagata, Y. Takagi, Y. Yoneda and T. Takenaka, *Appl. Phys. Express* **13**, 061002 (2020).
- 11) Y. Takagi, T. Miura, H. Nagata and T. Takenaka, *Jpn. J. Appl. Phys.* **58**, SLLD02 (2019).
- 12) Y. Takagi, H. Nagata and T. Takenaka, *J. Asian Ceram. Soc.* **8**, 277 (2020).
- 13) K. Eguchi, Y. Takagi, H. Nagata and T. Takenaka, *Jpn. J. Appl. Phys.* **59**, SPPD03 (2020).
- 14) Y. Takagi, K. Eguchi, H. Nagata, I. Sakaguchi and T. Takenaka, *J. Ceram. Soc. Jpn.* **129**, 383 (2021).
- 15) Y. Takagi, Y. Ochiai, M. Ito, T. Kawagoe, H. Nagata and I. Sakaguchi, *Jpn. J. Appl. Phys.* **61**, SN1034 (2022).
- 16) Y. Takagi, Y. Ochiai and H. Nagata, *Jpn. J. Appl. Phys.* **60**, SFFD02 (2021).
- 17) H. Nagata, T. Watanabe, Y. Hiruma and T. Takenaka, *Ferroelectrics* **404**, 2732 (2010).
- 18) S. Kawada, M. Kimura, Y. Higuchi and H. Takagi, *Appl. Phys. Express* **2**, 111401 (2009).
- 19) L. Gao, H. Guo, S. Zhang and C. Randall, *Actuators* **5**, 8 (2016).
- 20) T. B. Reed, "Free Energy of Formation of Binary Compounds", MIT Press, Cambridge, MA (1971).
- 21) I. Karakaya and W. T. Thomspon, *Bull. Alloy Phase Diagr.* **9**, 237 (1988).
- 22) V. Nguyen, H. Han, H. Lee, J. Yoon, K. Ahn and J. Lee, *J. Ceram. Process. Res.* **2**, s282 (2012).
- 23) N. Iwagami, H. Nagata, I. Sakaguchi and T. Takenaka, *J. Ceram. Soc. Jpn.* **124**, 644 (2016).
- 24) M. V. Slinkina, G. I. Dontsov and V. M. Zhukovsky, *J. Mater. Sci.* **28**, 5189 (1993).
- 25) H. Nagata, H. Haneda, I. Sakaguchi, T. Takenaka and J. Tanaka, *J. Ceram. Soc. Jpn.* **105**, 805 (1997).
- 26) C. Ahn, H. Song and S. Nahm, *J. Am. Ceram. Soc.* **89**, 921 (2006).
- 27) S. Kakroo, A. Kumar, S. K. Mishra, V. Singh and P. K. Singh, "Phase Transit.", Taylor & Francis (2016) p. 1063631.
- 28) G. Yesner, *J. Am. Ceram. Soc.* **101**, 5315 (2018).
- 29) J. Lv, T. Karaki and M. Adachi, *Jpn. J. Appl. Phys.* **49**, 09MD06 (2010).
- 30) G. Yesner, M. Kuciej and A. Safari (2015). doi:10.1109/ISAF.2015.7172658
- 31) M. Difeo, L. Ramajo and M. Castro, *J. Adv. Dielectr.* **11**, 2140004 (2021).
- 32) H. Y. Tian, K. W. Kwok, H. L. W. Chan and C. E. Buckley, *J. Mater. Sci.* **42**, 9750 (2007).
- 33) F. Zhang, X. Qiao, Q. Shi, X. Chao, Z. Yang and D. Wu, *J. Eur. Ceram. Soc.* **41**, 368 (2021).
- 34) W. Jo, J. Ollagnier, J. Park, E. Anton, O. Kwon, C. Park, H. Seo, J. Lee, E. Erdem, R. Eichel and J. Rödel, *J. Eur. Ceram. Soc.* **31**, 2107 (2011).
- 35) C. Ahn, H. Kim, W. Woo, S. Won, H. Seog, S. Chae, B. Park, K. Jang, Y. Ok, H. Chong and I. Kim, *J. Am. Ceram. Soc.* **98**, 1877 (2015).

- 36) C. Chou, C. Liu, C. Hsiung and R. Yang, *Powder Technol.* **210**, 212 (2011).
- 37) J. Kang, D. Heo, V. Nguyen, H. Han and J. Lee, *J. Korean Phys. Soc.* **61**, 899 (2012).
- 38) C. Lee, H. Han, S. Kim, T. Dinh, C. Ahn and J. Lee, *J. Electroceram.* **41**, 4349 (2018).
- 39) V. Schmitt and F. Raether, *J. Eur. Ceram. Soc.* **34**, 1521 (2014).
- 40) T. Kujirai, Y. Takagi, H. Nagata and T. Takenaka (2019). doi:10.1109/ISAF43169.2019.9034936
- 41) H. Park, J. Choi, M. Choi, K. Cho and S. Nahm, *J. Am. Ceram. Soc.* **91**, 2374 (2008).
- 42) H. Han, J. Koruza, E. Patterson, J. Schulthei, E. Erdem, W. Joc, J. Leed and J. Rödel, *J. Eur. Ceram. Soc.* **37**, 2083 (2017).
- 43) M. Matsubara, T. Yamaguchi, K. Kikuta and S.-I. Hirano, *Jpn. J. Appl. Phys.* **43**, 7159 (2004).
- 44) M. Matsubara, T. Yamaguchi, W. Sakamoto, K. Kikuta, T. Yogo and S.-I. Hirano, *J. Am. Ceram. Soc.* **88**, 1190 (2005).
- 45) J. B. Lim, S. Zhang, J.-H. Jeon and T. R. Shrout, *J. Am. Ceram. Soc.* **93**, 1218 (2010).
- 46) D. Lin, K. W. Kwok and H. L. W. Chan, *Appl. Phys. Lett.* **90**, 232903 (2007).
- 47) S.-L. Yang, C.-C. Tsai, Y.-C. Liou, C.-S. Hong, B.-J. Li and S.-Y. Chu, *J. Am. Ceram. Soc.* **93**, 1011 (2012).
- 48) R. M. German, P. Suri and S. J. Park, *J. Mater. Sci.* **44**, 139 (2009).
- 49) H. Wang, Y. Dai and X. Zhang, *J. Am. Ceram. Soc.* **95**, 1182 (2012).
- 50) Q. Chen, L. Chen, Q. Li, X. Yue, D. Xiao and J. Zhu, *J. Appl. Phys.* **102**, 104 (2007).
- 51) C. Chou, C. Liu, C. Hsiung and R. Yang, *Powder Technol.* **210**, 212 (2011).
- 52) M. Humenik and N. M. Parikh, *J. Am. Ceram. Soc.* **3**, 3960 (1956).
- 53) Y. Imanaka, "Multilayered Low Temperature Cofired Ceramics (LTCC) Technology", Springer Science, Dordrecht, The Netherlands (2005).
- 54) K. Ojima, K. Iwasaki, Y. Takagi and H. Nagata, *J. Ceram. Soc. Jpn.* **131**, 209 (2023).
- 55) M. Li, M. J. Pietrowski, R. A. De Souza, H. Zhang, I. M. Reaney, S. N. Cook, J. Kilner and D. C. Sinclair, *Nat. Mater.* **13**, 31 (2014).
- 56) F. Lu, F. Fang and Y. Chen, *J. Eur. Ceram. Soc.* **21**, 1093 (2001).
- 57) A. D. Pelton, *Bull. Alloy Phase Diagr.* **7**, 2527 (1986).